ACS Catalysis

Research Article

pubs.acs.org/acscatalysis

Simultaneous Orthogonal Methods for the Real-Time Analysis of Catalytic Reactions

Robin Theron,[†] Yang Wu,[†] Lars P. E. Yunker,[†] Amelia V. Hesketh,[†] Indrek Pernik,[‡] Andrew S. Weller,[‡] and J. Scott McIndoe*[,†]

[†]Department of Chemistry, University of Victoria, P.O. Box 3065 Victoria, British Columbia V8W3 V6, Canada

[‡]Department of Chemistry, University of Oxford, Mansfield Road, Oxford OX1 3TA, United Kingdom

Supporting Information

ABSTRACT: Continuous monitoring of catalyzed reactions using infrared spectroscopy (IR) measures the transformation of reactant into product, whereas mass spectrometry delineates the dynamics of the catalytically relevant species present at much lower concentrations, a holistic approach that provides mechanistic insight into the reaction components whose abundance spans 5 orders of magnitude. Probing reactions to this depth reveals entities that include precatalysts, resting states, intermediates, and also catalyst impurities and decomposition products. Simple temporal profiles that arise from this analysis aid discrimination between the different types of species, and a hydroacylation reaction catalyzed by a cationic rhodium complex is studied in detail to provide a test case for the utility of this methodology.

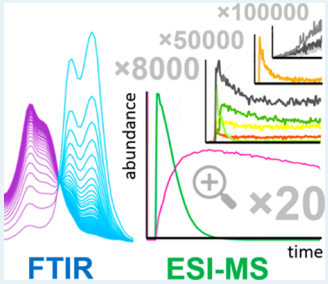

KEYWORDS: *mass spectrometry, infrared spectroscopy, real-time monitoring, catalysis, hydroacylation*

Catalytic reactions are notoriously difficult to study directly under real reaction conditions, principally because the abundance of the catalyst is typically several orders of magnitude lower than that of the substrates. For example, a 1 mol % catalyst loading is at the limit of sensitivity for standard in situ NMR experiments. Although more sophisticated nuclear spin polarization methods can produce remarkable enhancements to signals (10^2−10^4) in NMR spectroscopy, such techniques are generally equipment and/or catalyst system specific.[1] Few available, straightforward techniques are sensitive enough to determine the catalyst speciation while at the same time not being overwhelmed by the large quantities of substrate, products, and solvent present, though the combination of multiple methods is becoming an increasingly popular solution.[2] The high dynamic range of electrospray ionization mass spectrometry (ESI-MS) enables detection of otherwise-invisible, catalytically relevant species,[3] and pressurized sample infusion (PSI) provides a methodology to allow for continuous monitoring of catalytic reactions.[4] However, when using ESI-MS to monitor substrates and products, the catalytic species observed are for the most part the resting state and/or the most abundant on-cycle species. This does not utilize the full potential of ESI-MS to probe deeper into even less abundant species, because the concentration range employed does not exercise the sensitivity limits of the instrument. The ideal approach would be to co-opt some other, less sensitive, orthogonal technique to monitor overall reaction progress, while using the ESI-MS to focus exclusively on the low abundance, catalytically relevant species. Infrared spectroscopy (IR) is the perfect complementary tool for this (especially under flow conditions), but it comes with certain reaction design criteria for monitoring by flow IR/ESI-MS: (1) an IR spectroscopic handle in substrates/products; (2) a cationic catalyst, appropriate reaction times and catalysis concentrations (minutes to hours, catalyst at low mol % level; a charged catalyst circumvents the need for charge-tagging strategies);[5] (3) atom efficiency so products and substrates reciprocally track each other. The catalyzed hydroacylation reaction (the potentially 100% atom efficient C−H activation/C−C coupling between an aldehyde and olefin to form a ketone) offers an ideal platform to develop flow IR/ESI-MS as it is commonly catalyzed by well-defined cationic Rh−phosphine systems at low catalyst loadings (0.1−5 mol %), and has the benefit of an aldehyde to ketone transformation which have well-defined IR-reporter carbonyl groups.[6]

Catalytic chemists have always had strong intuitions about the temporal evolution of various components of a reaction (Figure 1) and especially the temporal evolution of reactants and products.[7] They expect reactant to be consumed and product to be formed that follow zero-, first-, or second-order kinetics (and sometimes more complex kinetics). Many methods, spectroscopic and otherwise, exist to establish these data.[8] However, given that ESI-MS is able to probe temporal evolution of species at concentration levels several orders of magnitude lower than most other techniques, it is worth thinking about what behaviors might be expected to be observed of species directly or indirectly related to the precatalyst (Figure 1). The precatalyst itself might be expected to diminish at a rate related to the initiation period. Species that

Received: May 27, 2016
Revised: July 30, 2016
Published: September 1, 2016

DOI: 10.1021/acscatal.6b01489
ACS Catal. 2016, 6, 6911−6917

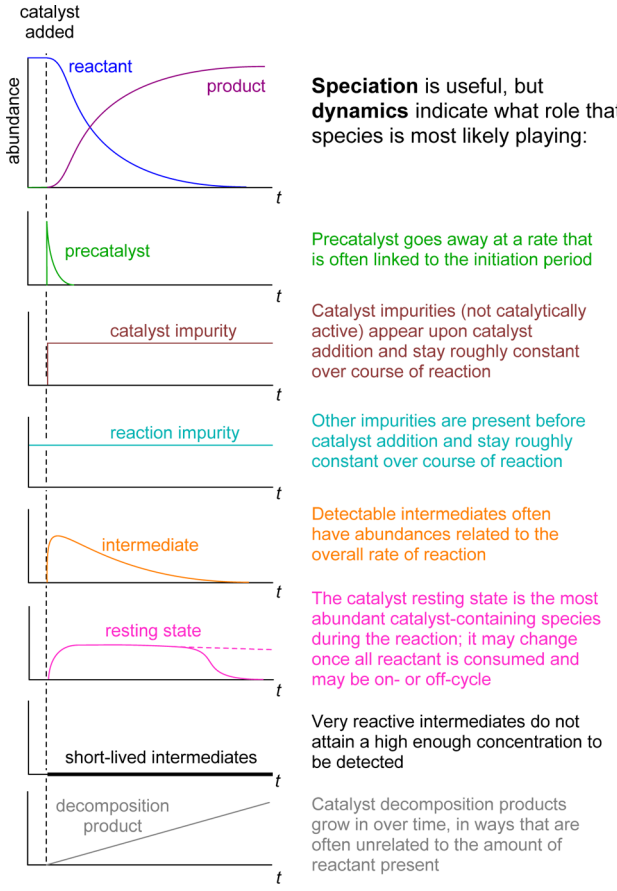

Figure 1. Idealized dynamic behavior for various reaction components over the course of a reaction.

grow in over time and whose production is independent of substrate or product concentration can be quickly identified as decomposition products.[6b] Species that have a non-zero concentration at time = zero and whose abundance is largely unaffected as the reaction proceeds are most likely impurities or cross-contaminants. Species that track, in some form, substrate and product relative concentrations are the best candidates for participating in the catalytic cycle, either as transient intermediates that are substrate concentration dependent or persistent resting states (for example, strong product−binding to the catalyst).[5] Off-cycle species that are not decomposition products, such as inactive dimers that reversibly form monomeric active species[9] or species that derive from changing concentrations of reactants and products,[10] may be affected by overall reaction progress depending on the equilibria involved. In this contribution, we demonstrate many of these temporal speciation profiles can be observed for substrates, products, and the very low relative concentrations of species related to the catalyst for the hydroacylation reaction of 1-octyne and the aldehyde 2-(methylthio)benzaldehyde as catalyzed by a cationic rhodium catalyst $[Rh(L)(\eta^6\text{-PhF})][BAr^F{}_4]$ [L = $MeN(P^iPr_2)_2$, Ar^F = 3,5-$C_6H_3(CF_3)_2$]. This serves to benchmark the IR/ESI-MS technique as one that has potential to be of broad applicability in the study of homogeneous catalytic processes.

RESULTS

The hydroacylation of 1-octyne (**2**) and the aldehyde 2-(methylthio)benzaldehyde (**1**) as catalyzed by a cationic rhodium catalyst $[Rh(L)(\eta^6\text{-PhF})][BAr^F{}_4]$[11] **4**$[BAr^F{}_4]$ was studied using flow FTIR in 1,2-$C_2H_4Cl_2$ solvent to measure the overall progress of reaction (tracking the disappearance of aldehyde **1** and the appearance of ketone **3**, see Supporting Information Figures S3 and S4 for more details) while also employing PSI-ESI-MS to measure the temporal evolution of catalytically relevant species (Figure 2). This catalyst has been shown to give a good linear/branched ratio of the resulting α,β-unsaturated ketone product (21:1) that simplifies the analysis of the reaction.

NMR spectroscopy delivers no useful information at 298 K because at concentrations required to observe the organometallic species (10 mol %), the reaction is over before the first measured point.[11] At 193 K, the observed resting state is the product bound to $[Rh(L)]^+$, i.e. $[Rh(MeN(P^iPr_2)_2)(\kappa^2\text{-O,S-}CO(C_6H_4SMe)(CH{=}CH(CH)_5Me)][BAr^F{}_4]$, and under these conditions of catalyst turnover, no acyl hydride is observed, a likely intermediate that precedes the resting state. Such a species can be observed in low-temperature stoichiometric experiments but rapidly decays to a reductive decarbonylation decomposition product at room temperature, $[Rh(L)(SMePh)(CO)][BAr^F{}_4]$. The catalyst will also work at 1 mol %, but this is below the limit of sensitivity for routine NMR spectroscopy under the temporal conditions required for monitoring the progress of the reaction, and no catalytically relevant species can be observed.[5] Thus, NMR spectroscopy provides some information on the progress of the reaction, but catalyst speciation is limited to the product-bound resting state.

The experimental setup to reveal these species under these lower catalyst loadings is conceptually simple: a pressurized flask has a capillary emerging through a septum and attached to the mass spectrometer. The pressure is set to generate a flow rate suitable for regular ESI-MS analysis (~10 μL min^{-1}). Simultaneously, the reaction solution is circulated through an external IR flow cell (see Figure S2 for photograph of the setup). The IR data show clearly the disappearance of the aldehyde and generation of the ketone. The isosbestic points reveal that the reaction is a clean conversion of **1** → **3**.

Ten replicates with a 16 s scan time over 10 min revealed a highly reproducible, fast, first-order reaction with a half-life of 62 ± 7 s (k = 0.011 ± 0.001 s^{-1}, Figure 3). Such a time scale makes it difficult to reliably obtain sufficient data density to study the progress by standard NMR spectroscopic techniques.

Having left the IR to take care of the gross solution changes at the millimolar level, we can turn the analysis of low concentration, catalytically relevant species over to PSI-ESI-MS. The reaction is initiated by injection of a solution of the charged catalyst, **4**, and within 20 s its presence is registered by the ESI-MS (the time it takes for the solution to move through the capillary). The first species to appear is the catalyst precursor itself, $[Rh(L)(\eta^6\text{-PhF})]^+$ (**4**). It is rapidly consumed, disappearing almost completely within about 4 min, and is largely replaced by $[Rh(MeN(P^iPr_2)_2)(\kappa^2\text{-O,S-CO}(C_6H_4SMe)(CH{=}CH(CH)_5Me)]^+$ (**7**). This is as previously observed by NMR spectroscopy at high catalyst loadings (10 mol %) as the resting state.[5] Identification of this species during catalysis as being the product-bound catalyst was confirmed by comparing the MS/MS of the compound made when the product **3** was mixed with the precatalyst **4** independently (see S12). The traces in Figure 4 were averaged from seven different runs, four of which were run simultaneously with the IR analysis. Figure 5 presents the graphical representation of these species observed, as related to the proposed catalytic cycle.

DOI: 10.1021/acscatal.6b01489
ACS Catal. 2016, 6, 6911−6917

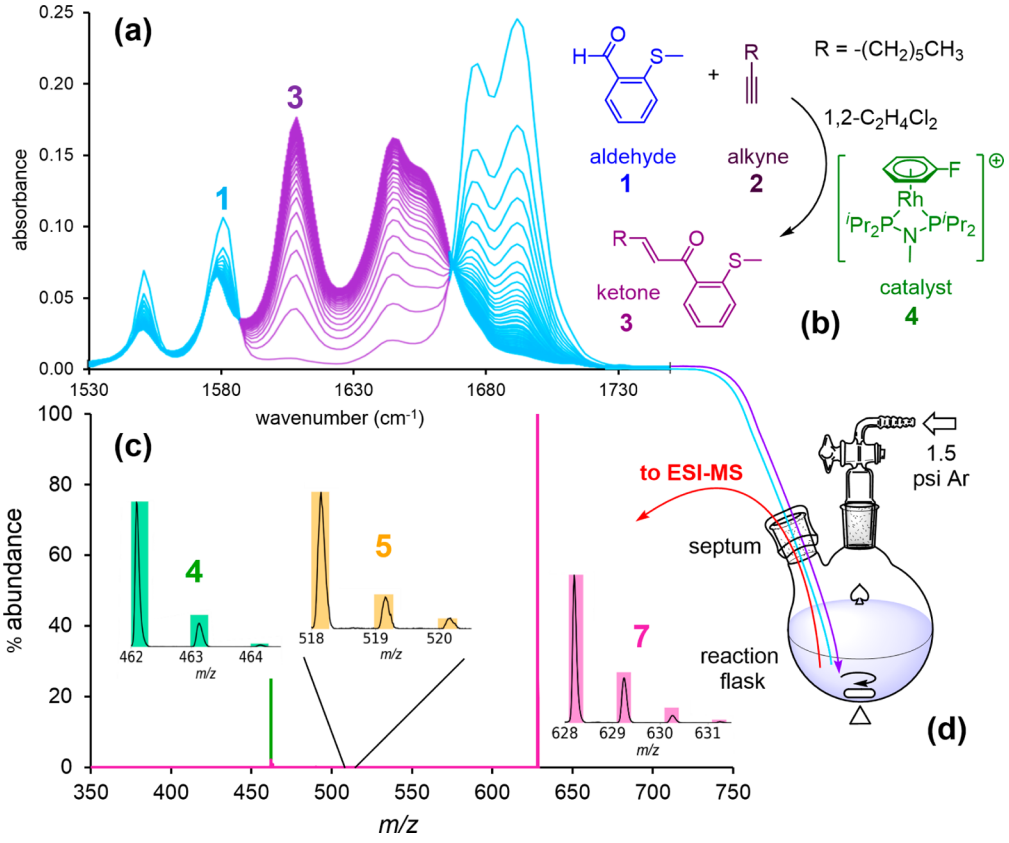

Figure 2. (a) IR spectral changes; (b) hydroacylation reaction under study: 0.075 M aldehyde **1**, 0.1125 M alkyne **2**, 5% catalyst **4**[BAr^F_4], 1,2-$C_2H_4Cl_2$ solvent, 22 °C. Reaction run to completion (^{1}H NMR at the end of the reaction shows the aldehyde is no longer present); (c) ESI-MS spectrum at t = 2 min. Inset shows calculated and actual isotope pattern of one of the intermediates; (d) Schematic of the instrumental setup. The blue/purple lines circulate the reacting solution through the IR flow cell at 1 mL/min. The red line pumps solution via pressurized sample infusion (PSI) directly into the mass spectrometer at ~10 μL min^{-1}.

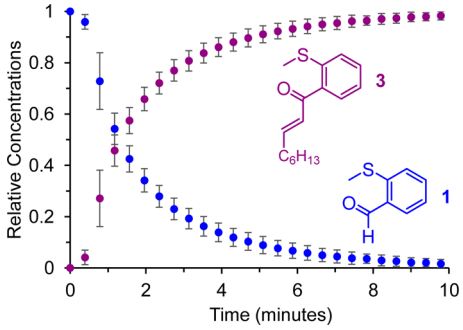

Figure 3. Concentration vs time profile for aldehyde and ketone. Error bars show standard deviations (10 replicates).

PSI-ESI-MS is quite capable of collecting real-time data on catalyst resting states while *also* collecting information on overall reaction progress if the substrate is charge-tagged.[12] However, this requires running the experiment at the low substrate concentrations (millimolar), which is a very high concentration for ESI-MS purposes.[13] Avoiding saturation and suppression effects at this concentration requires careful selection of experimental conditions and running at high substrate concentrations is not feasible.[14] As such, a dynamic range of only ~2−3 orders of magnitude is possible. Modern mass spectrometers run at more appropriate concentrations (micromolar and below) are capable of dynamic ranges of 3−5 orders of magnitude, but to harness these capabilities in a catalytic context requires some other technique to handle the overall progress of the reaction. By leaving the IR to take care of substrate and product concentrations, we can therefore delve deeper into the catalytic cycle: beyond the catalyst resting states to measure the low abundance species in real time. So what appears when we mine still further? Descending into the baseline (<1% of that shown in Figure 4b), we find rich dynamic behavior (Figure 4c). The most abundant trace in this plot is of [Rh(L)(MeSPh)]$^+$ (**8**) which is the expected decarbonylation product as well as [Rh(L)(O) (cyclooctadiene)]$^+$ (**9**), an oxidized impurity that presumably arises from the synthesis of **4**[BAr^F_4]. These two compounds could not be resolved as their exact masses differ by 0.06 Da, but by MS/MS analysis the species shows two clear pathways of dissociation corresponding to the two different compounds, with **8** being the predominant species (S14). The persistence of **8** in the trace suggests that the MeSPh generated in the formation of **8** remains in solution to continue to compete for coordination to the rhodium. Two of the other species are easily identified catalyst impurities, both present at less than 0.5% of the starting catalyst concentration. [Rh(L)(η^6-benzene)]$^+$ (**10**) arises from trace benzene impurity in the fluorobenzene, and it binds much more strongly to rhodium than PhF does.[15] [Rh(L) (cyclooctadiene)]$^+$ (**11**) likely comes from the synthesis of **4**[BAr^F_4], for which **11** is a precursor. Deliberate addition of one equivalent of cyclooctadiene to the reaction mixture prior to adding catalyst results in abundant formation of **11** (S17), and the reaction is considerably slower.

DOI: 10.1021/acscatal.6b01489
ACS Catal. 2016, 6, 6911−6917

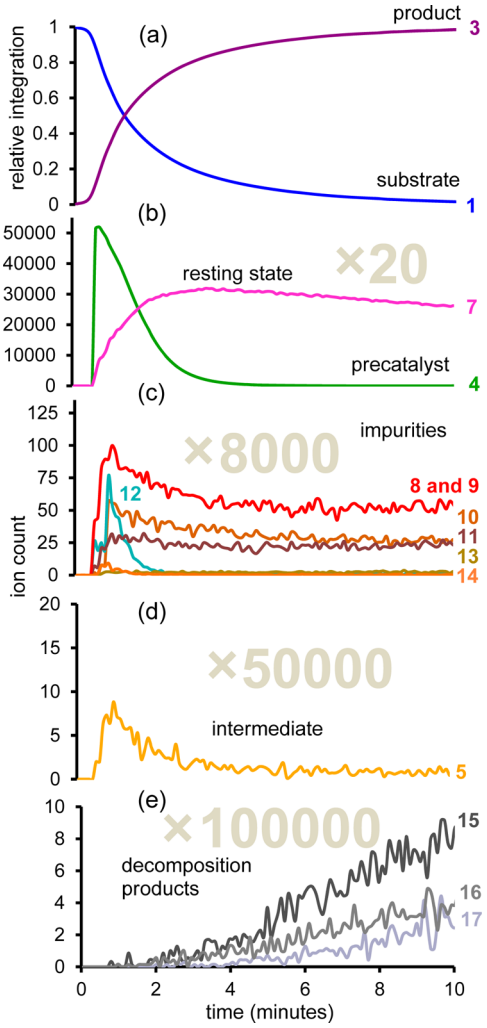

Figure 4. Real-time abundances from IR of (a) substrate and product, and from PSI-ESI-MS; (b) precatalyst and resting state; (c) catalyst impurities (both poisoned and active precatalysts) and off-cycle species; (d) intermediate; (e) catalyst decomposition products. Estimated concentrations span from 0.07 M down to parts-per-million. An animated version of these data is available in Supporting Information as a short movie.

The species at m/z 433.1 (**12**) and around m/z 478 (**13** and **14**) were initially a puzzle. The ion at m/z 433.1 (**12**) exhibited intensity that varied considerably from one experiment to the next. Its behavior under MS/MS conditions was consistent with an ion of the form $[Rh(L)(neutral)]^+$, where neutral has a mass of 67.09 Da, corresponding to C_4H_5N. There are few molecules with this formula, pyrrole being the most commonly encountered, and MS/MS of the m/z 433.1 ion generated when pyrrole is mixed with **4** closely resembles that of the species we observe during catalysis (S19). Neither pyrrole nor any other C_4H_5N molecule are reagents we use in the laboratory. The most likely source of the pyrrole is as a stabilizer in the $C_2H_4Cl_2$ solvent, for which it is an antioxidant preventing decomposition reactions.[16] **12** does however go away quickly during the reaction, being almost entirely consumed within 2 min, suggesting that the neutral molecule is weakly bound and easily displaced by a stronger ligand (the product, resulting in **7**). As such, its profile closely resembles that of the $[Rh(L)(\eta^6\text{-PhF})]^+$ (**4**) precatalyst. There are two signals that display contrasting behavior at m/z 477.2 and m/z 478.1. The peak at m/z 477.2, **13**, displays the characteristics of a tenaciously bound impurity, as its dynamic behavior is very similar to the cyclooctadiene and benzene complexes. The additional mass over and above that of $[Rh(L)]^+$ of 111.1 Da corresponds to $C_7H_{13}N$, for which there are a large number (hundreds) of possible compounds, including heptanonitrile, quinuclidine, pyrrolizidine, and methyldiallylamine. Given the dissimilarity of the behavior of this impurity compared to the pyrrole complex, all we can really say about this compound is that it is most likely not a secondary amine. The peak at m/z 478.1, **14**, disappears rapidly, fragments by loss of a neutral mass of 96 Da (almost certainly fluorobenzene) and probably represents an oxidized form of the precatalyst (loss of 96 Da leaves $[Rh(L)O]^+$). Most likely, the oxygen has oxidized one of the phosphorus atoms of the ligand to leave a chelating bisphosphinemonoxide.[17]

Drilling still deeper into the baseline, at approximately 1/50 000th of the abundance of the substrate, we observe a trace that is especially interesting because its abundance tracks very closely with the overall rate of reaction (Figure 4d). It is most abundant when the reaction is fastest and drops to zero upon exhaustion of the substrate. This corresponds to intermediate **5**, which is the product of oxidative addition of the aldehyde to form a reactive acyl hydride, $[Rh(L)(H)(MeSC(O)C_6H_4)]^+$. Again, at these loadings, the concentration and the temporal requirements of the reaction mean that NMR spectroscopy cannot capture this intermediate; although they can been observed under stoichiometric conditions, using these and related systems, stabilized by coordination of a Lewis base (such as acetone or NCMe).[4,5] A final collection of low-abundance compounds steadily accumulate for the 10 min of reaction, suggesting decomposition products (Figure 4e). One involves overall addition of two Cl atoms (which have a characteristic effect on the isotope pattern) (**15**) and likely arises from reaction with the solvent, 1,2-$Cl_2C_2H_4$, and **16** involves additional alkyne, presumably from a subsequent carbothiolation[18] of the product ketone with another alkyne. **16** is in turn susceptible to O_2 addition to form **17**.

The reproducibility of the traces obtained through PSI-ESI-MS varied depending on their abundance. For the most abundant species, **4** and **7**, the traces matched each other well across all seven runs (see Figure S10). However, as the abundance dropped, percentage variability in each signal increased (see Figure S22). This observation was predictable; the low abundance species are most likely to be affected by fluctuations in impurity levels due to solvent contamination, trace amounts of O_2, and so on.

DISCUSSION

With the power of modern instrumentation working in tandem on aspects of measurement to which they are best suited, the accepted wisdom "if you can see something during a catalytic reaction, it is not an intermediate" is weakening.[19] However, this study has revealed more than was initially intended: when probing speciation at very low concentration, the analyst has to accept that species other than those thought to have been added may also be detectable.

So what does the "at-a-glance" approach outlined in Figure 1 tell us about the mechanism of the reaction under study here? Figure 5 shows the proposed catalytic cycle based on previous work, elaborated to include the off-cycle species and impurities.

The IR data reveals that the reaction is clean and produces minimal byproducts, and that it is first-order overall under the

DOI: 10.1021/acscatal.6b01489
ACS Catal. 2016, 6, 6911−6917

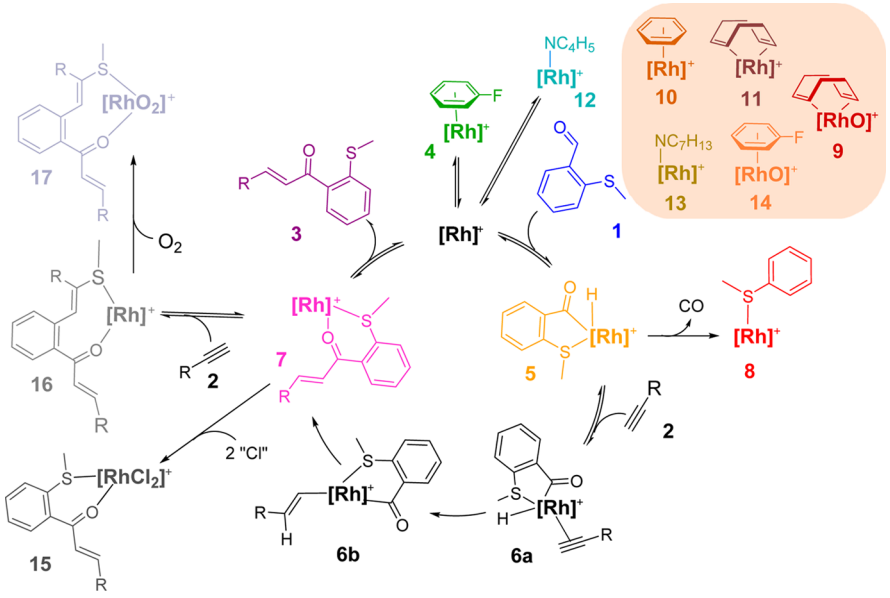

Figure 5. Catalytic cycle. Catalyst impurities boxed off. $[Rh]^+ = [Rh(L)]^+$ where L = $MeN(P^iPr_2)_2$. Color scheme correlates with Figure 4.

conditions used. The precatalyst is entirely consumed within minutes, and the resting state of the catalyst involves the product binding to the metal. A variety of catalyst impurities at the <1% level are observed and fall into two categories: poisoned catalysts (that do not change intensity over time) and precatalysts (with a different ligand set than the intended precatalyst but which display the same behavior). Decarbonylation products are observed at a low level, suggesting that the slight excess of alkyne used is successfully discouraging this unproductive pathway, which has been shown to operate when an excess of aldehyde is used.[5] The steady accumulation of decomposition products pointed toward the value of knowing exactly when the reaction is over by use of tandem infrared measurements—excess alkyne shuts down decarbonylation but introduces the risk of double insertion reducing the yield of desired product, and there are no signs of this rate diminishing once all of the aldehyde was consumed.

Intermediates **6a**, **6b**, and **7** all have the same m/z value and are hence indistinguishable by ESI-MS mass spectrometry. **6a** and **6b** may well contribute to the signal dominated by **7** but not sufficiently to provide evidence in the MS/MS spectrum. We would expect loss of 110.1 Da, corresponding to octyne **2** in the case of **6a.** What we see in the MS/MS spectrum is clean loss of the product, **3** (262.5 Da, see Supporting Information Figure S11), suggesting that the carbon−carbon bond-forming reaction has already occurred and we are indeed observing **7**. Note however that it is possible that **6b** prefers to decompose by reductive elimination and ligand dissociation rather than by β-elimination of the alkyne, in which case its MS/MS spectrum will resemble that of **7**.

The on-cycle, resting state intermediate **7** is consistent with previous observations from NMR spectroscopy, in which D-labeling experiments also show that β-hydrogen elimination from vinyl intermediate **6b** is unlikely.[5] In addition, for a $\{Rh(DPEphos)\}^+$ system kinetic modeling and labeling experiments support that the hydride insertion is also irreversible,[20] although in this system, reductive C−C coupling is turnover limiting. Reversible hydride insertion into alkynes is rare.[21] These observations combine to suggest that **7** is the resting state. Under this assumption that hydride insertion into the alkyne is irreversible, the observation of a species consistent with acyl-hydride **5** as an intermediate, rather than **6b**, suggests that it precedes the turnover-limiting step. Initial-rate studies at loadings of 1 mol % using NMR spectroscopy showed a positive order on the alkyne,[11] suggesting reversible binding of this substrate prior to the turnover-limiting step, while a relatively small kinetic isotope effect (KIE) when deutero(**1**) is used (1.6 ± 0.2) that suggests that irreversible aldehyde oxidative addition is not turnover-limiting. This measured KIE could be consistent with **6a** to **6b** being turnover limiting (i.e., hydride insertion). Such a scenario has been suggested to be occurring in salicylaldehyde alkene hydroacylation,[22] while the small KIE measured is similar to that proposed for the hydride migration step in the hydroformylation of 1-octene.[23] Hofmann and co-workers have demonstrated increased barriers to alkyl migration in related small bite angle systems,[24] consistent with this scenario. Hydride insertion being turnover limiting in this alkyne hydroacylation is in contrast to alkene hydroacylation using aldehyde **1** and small-bite angle diphosphine Rh-catalysts in which fast and reversible hydride insertion is indicated.[4] We have previously used ESI−MS/MS to study the temporal evolution of a slow (∼1 h) *stoichiometric* hydroacylation reaction between **1** and methyl acrylate using $[Rh(DPEphos)]^+$-based catalysts, which shows an intermediate species assigned as the species that follows hydride insertion but precedes reductive elimination (i.e., the analogue of **6b**). As is becoming increasingly apparent, the turnover-limiting step, as well as the reversibility of hydride insertion, is very system- and substrate-dependent in hydroacylation.

Of the substances assigned as catalyst impurities, **11**, the COD complex, displays the most ideal behavior (a near perfect step-function). **8** and **9** overlap, and it is quite possible that the trace in Figure 4c is a composite of **8** slowly diminishing (e.g., displacement of the monodentate ligand by **3**) while **9** stays steady. **10** also shows some slight diminishment over time, perhaps also through slow displacement by a better ligand (e.g., **3**).

ESI-MS is of course blind to neutral species, and while this is convenient in the sense that the catalytic species are not overwhelmed by the vastly more abundant solvent, substrate,

DOI: 10.1021/acscatal.6b01489
ACS Catal. 2016, 6, 6911−6917

and product, it does mean that the method will not detect any reduced, Rh(0) complexes, and signal-to-noise considerations also prevent the detection of nanoparticles.

CONCLUSIONS

There are certain fundamental questions which chemists studying catalytic mechanisms want answers. What is the turnover-limiting step? How is the catalyst dying? What are the catalyst resting states? What are the intermediates? Is this species observed spectroscopically relevant to the catalytic cycle? The application of multiple real-time orthogonal techniques to this sort of problem, especially when one of them is as sensitive as ESI-MS, offers the most profound answers to these questions to date. The possibility of using other spectroscopic methods with ESI-MS to provide similarly powerful insights is an obvious extension in cases where reactions lack a suitable FTIR handle.

METHODS

General. All reactions were performed under nitrogen or argon using Schlenk technique or in an inert atmosphere glovebox (MBraun LabMaster 130). Dichloromethane and hexane were HPLC grade and purified by an MBraun solvent purification system. Fluorobenzene and 1,2-dichloroethane were dried over calcium hydride, distilled, then stored over 4 Å molecular sieves. 2-(Methylthio)benzaldehyde (**1**) was prepared according to a literature method[25] and vacuum distilled prior to use. The rhodium precatalyst **4**[BAr^F_4] was prepared according to a literature method.[5] 1-Octyne (**2**) was dried over calcium hydride and distilled before use. All other chemicals were purchased from Sigma-Aldrich and used without further purification.

Monitoring by IR. IR measurements were done on a Bruker Alpha FT-IR fitted with a Harrick demountable transmission flowcell with BaF_2 windows, a 100 μm path length, and a 5 μL cell volume. The reaction solution was circulated through the flow cell via tubing of 250 μm inner diameter using a Simdos 02 Pump at a flow rate of 2.5 mL/min. A background of 1,2-dichloroethane was collected prior to each experiment, after which the pump was purged with argon before introducing reaction solution.

Monitoring by ESI-MS. ESI-MS measurements were done on a Micromass Q-Tof *micro* mass spectrometer in positive ion mode using pneumatically assisted electrospray ionization: scan time 1 s; capillary voltage 2900 V; sample cone voltage 15 V; extraction voltage 0.5 V; source temperature 84 °C; desolvation temperature 184 °C; cone gas flow 100 L/h; desolvation gas flow 200 L/h; collision voltage 2 V; MCP voltage 2400 V. Reaction solution was continually fed from the reaction flask into the mass spectrometer via 125 μm inner diameter PEEK tubing. Spectral assignment was aided by the free tools available at chemcalc.org.[26] Intensity versus time traces in the paper were assembled from averages of seven independent runs carried out over a period of several months to ensure reproducibility.

Typical IR-MS Reaction Procedure. An overpressure of 2 psi of argon gas was applied to a Schlenk flask containing 1,2-dichloroethane. The flask was connected to the inlet of the circulation pump by PEEK tubing, the outlet of the circulation pump was connected to the entrance of the IR flow-cell, and the outlet of the flow cell was connected via tubing to a waste flask. The pump was turned on, and the solvent was run through the pump and flow cell into the waste flask. After 2 mL of solvent had passed through the system, the exit tubing from the flow-cell was inserted into the Schlenk flask, creating a continuous loop. A background IR spectrum of solvent circulating through the flow-cell was collected. The solvent was purged from the flask by removing the exit tubing and placing it into a waste flask. After all the solvent had been removed and the system purged with argon, the exit tubing was reinserted into the Schlenk flask. A solution of 2-(methylthio)-benzaldehyde (90 mmol/L, 0.225 mmol) and 1-octyne (135 mmol/L, 0.338 mmol) in 1,2-dichloroethane (2.5 mL) was added to the argon filled Schlenk flask. The flask was connected to the mass spectrometer via a short length of PEEK tubing and mass spectra collection was initiated followed by initiation of collection on the IR spectrometer. A solution of $[Rh(L)(FPh)]^+$ $[BAr^F_4]^-$ in 1,2-dichloroethane (0.5 mL, 22.5 mmol/L, 0.0113 mmol) was injected into the pressurized Schlenk flask through the septum, while the solution was well stirred, and this commenced the reaction.

ASSOCIATED CONTENT

Supporting Information

The Supporting Information is available free of charge on the ACS Publications website at DOI: 10.1021/acscatal.6b01489.

Further experimental details, IR spectra, calibration curves, kinetic data, and MS/MS data (PDF)

Animated video of the data presented in Figure 4 (MPG)

AUTHOR INFORMATION

Corresponding Author

*E-mail: mcindoe@uvic.ca. Fax: +1 (250) 721-7147. Tel: +1 (250) 721-7181.

Notes

The authors declare no competing financial interest.

ACKNOWLEDGMENTS

J.S.M. thanks Natural Sciences and Engineering Research Council (Discovery and Discovery Accelerator Supplement) for operational and infrastructural funding and the Canada Foundation for Innovation, BC Knowledge Development Fund, and the University of Victoria for infrastructural support. The Royal Society for an International Exchange Award (ASW and JSM), Archimedes Foundation (Estonia) for a Ph.D. Scholarship (IP), EPSRC (ASW, EP/M024210/1).

REFERENCES

(1) (a) Cowley, M. J.; Adams, R. W.; Atkinson, K. D.; Cockett, M. C. R.; Duckett, S. B.; Green, G. G. R.; Lohman, J. A. B.; Kerssebaum, R.; Kilgour, D.; Mewis, R. E. *J. Am. Chem. Soc.* **2011**, *133*, 6134−6137. (b) Ardenkjær-Larsen, J. H.; Fridlund, B.; Gram, A.; Hansson, G.; Hansson, L.; Lerche, M. H.; Servin, R.; Thaning, M.; Golman, K. *Proc. Natl. Acad. Sci. U. S. A.* **2003**, *100*, 10158−10163.

(2) (a) Foley, D. A.; Doecke, C. W.; Buser, J. Y.; Merritt, J. M.; Murphy, L.; Kissane, M.; Collins, S. G.; Maguire, A. R.; Kaerner, A. *J. Org. Chem.* **2011**, *76*, 9630−9640. (b) Chanda, A.; Daly, A. M.; Foley, D. A.; LaPack, M. A.; Mukherjee, S.; Orr, J. D.; Reid, G. L., III; Thompson, D. R.; Ward, H. W. *Org. Process Res. Dev.* **2015**, *19*, 63−83. (c) Drexler, M. T.; Foley, D. A.; Ward, H. W., II; Clarke, H. J. *Org. Process Res. Dev.* **2015**, *19*, 1119−1127. (d) Strieter, E. R.; Bhayana, B.; Buchwald, S. L. *J. Am. Chem. Soc.* **2009**, *131*, 78−88. (e) Foley, D. A.; Wang, J.; Maranzano, B.; Zell, M. T.; Marquez, B. L.; Xiang, Y.; Reid, G. L. *Anal. Chem.* **2013**, *85*, 8928−8932.

(3) (a) Chen, P. *Angew. Chem., Int. Ed.* **2003**, *42*, 2832−2847. (b) Santos, L. S.; Rosso, G. B.; Pilli, R. A.; Eberlin, M. N. *J. Org. Chem.*

DOI: 10.1021/acscatal.6b01489
ACS Catal. 2016, 6, 6911−6917

2007, *72*, 5809−5812. (c) Roithová, J. *Chem. Soc. Rev.* **2012**, *41*, 547−559. (d) Yunker, L. P. E.; Stoddard, R. L.; McIndoe, J. S. *J. Mass Spectrom.* **2014**, *49*, 1−8. (e) Perry, R. H.; Splendore, M.; Chien, A.; Davis, N. K.; Zare, R. N. *Angew. Chem., Int. Ed.* **2011**, *50*, 250−254. (f) Schröder, D. *Acc. Chem. Res.* **2012**, *45*, 1521−1532. (g) Behrends, M.; Savmarker, J.; Sjoberg, P. J. R.; Larhed, M. *ACS Catal.* **2011**, *1*, 1455−1459. (h) Sabino, A. A.; Machado, A. H. L.; Correia, C. R. D.; Eberlin, M. N. *Angew. Chem., Int. Ed.* **2004**, *43*, 2514−2518.

(4) Vikse, K. L.; Woods, M. P.; McIndoe, J. S. *Organometallics* **2010**, *29*, 6615−6618.

(5) (a) Chisholm, D. M.; McIndoe, J. S. *Dalton Trans.* **2008**, 3933−3945. (b) Schade, M.; Fleckenstein, J. E.; Knochel, P.; Koszinowski, K. *J. Org. Chem.* **2010**, *75*, 6848−6857.

(6) (a) Willis, M. C. *Chem. Rev.* **2010**, *110*, 725−748. (b) Chaplin, A. B.; Hooper, J. F.; Weller, A. S.; Willis, M. C. *J. Am. Chem. Soc.* **2012**, *134*, 4885−4897. (c) Murphy, S. K.; Bruch, A.; Dong, V. M. *Angew. Chem., Int. Ed.* **2014**, *53*, 2455−2459. (d) Murphy, S. K.; Bruch, A.; Dong, V. M. *Angew. Chem.* **2014**, *126*, 2487−2491. (e) Castaing, M.; Wason, S. L.; Estepa, B.; Hooper, J. F.; Willis, M. C. *Angew. Chem., Int. Ed.* **2013**, *52*, 13280−13283. (f) Prades, A.; Fernández, M.; Pike, S. D.; Willis, M. C.; Weller, A. S. *Angew. Chem., Int. Ed.* **2015**, *54*, 8520−8524.

(7) (a) Hartwig, J. *Organotransition Metal Chemistry: From Bonding to Catalysis*; University Science Books: Herndon, VA, 2009. (b) van Leeuwen, P. W. N. M. *Homogeneous Catalysis Understanding the Art*; Springer: Berlin, 2004. (c) Bligaard, T.; Bullock, R. M.; Campbell, C. T.; Chen, J. G.; Gates, B. C.; Gorte, R. J.; Jones, C. W.; Jones, W. D.; Kitchin, J. R.; Scott, S. L. *ACS Catal.* **2016**, *6*, 2590−2602. (d) Garland, M.; Li, C.; Guo, L. *ACS Catal.* **2012**, *2*, 2327−2334. (e) Blackmond, D. G. *J. Am. Chem. Soc.* **2015**, *137*, 10852−10866. (f) Xu, Q.; Guo, L.; Dinh, T. D.; Cheong, A.; Garland, M. *ACS Catal.* **2015**, *5*, 3588−3599.

(8) (a) Yarwood, J.; Douthwaite, R.; Duckett, S. B. *Spectroscopic Properties of Inorganic and Organometallic Compounds*; RSC Publishing: Cambridge, 2010. (b) Grabow, K.; Bentrup, U. *ACS Catal.* **2014**, *4*, 2153−2164. (c) Torres, A.; Perez, N. M.; Overend, G.; Hodge, N.; Heaton, B. T.; Iggo, J. A.; Satherley, J.; Whyman, R.; Eastham, G. R.; Gobby, D. *ACS Catal.* **2012**, *2*, 2281−2289. (d) Selent, D.; Heller, D. In *Catalysis*; Beller, M., Renken, A., van Santen, R. A., Eds.; Wiley-VCH: Weinheim, Germany, 2012; pp 465− 492. (e) Jordan, R. B. *Reaction Mechanisms of Inorganic and Organometallic Systems*, 3rd ed.; Oxford University Press: New York, 2007; pp 422−456.

(9) (a) Fryzuk, M. D.; Piers, W. E.; Einstein, F. W. B.; Jones, T. *Can. J. Chem.* **1989**, *67*, 883. (b) Brown, J. M.; Lloyd-Jones, G. C. *J. Chem. Soc., Chem. Commun.* **1992**, 710. (c) Van Strijdonck, G. P. F.; Boele, M. D.; Kamer, P. C.; De Vries, J. G.; van Leeuwen, P. *Eur. J. Inorg. Chem.* **1999**, *1999*, 1073.

(10) (a) Renkema, K. B.; Kissin, Y. V.; Goldman, A. S. *J. Am. Chem. Soc.* **2003**, *125*, 7770. (b) Göttker-Schnetmann, I.; White, P.; Brookhart, M. *J. Am. Chem. Soc.* **2004**, *126*, 1804. (c) Göttker-Schnetmann, I.; Brookhart, M. *J. Am. Chem. Soc.* **2004**, *126*, 9330.

(11) Pernik, I.; Hooper, J. F.; Chaplin, A. B.; Weller, A. S.; Willis, M. C. *ACS Catal.* **2012**, *2*, 2779−2786.

(12) (a) Vikse, K. L.; Ahmadi, Z.; Manning, C. C.; Harrington, D. A.; McIndoe, J. S. *Angew. Chem., Int. Ed.* **2011**, *50*, 8304−8306. (b) Luo, J.; Oliver, A. G.; McIndoe, J. S. *Dalton Trans.* **2013**, *42*, 11312−11318. (c) Ahmadi, Z.; McIndoe, J. S. *Chem. Commun.* **2013**, *49*, 11488−11490.

(13) Cech, N. B.; Enke, C. G. *Mass Spectrom. Rev.* **2001**, *20*, 362−387.

(14) (a) Janusson, E.; Hesketh, A. V.; Bamford, K. L.; Hatlelid, K.; Higgins, R.; McIndoe, J. S. *Int. J. Mass Spectrom.* **2015**, *388*, 1−8. (b) Pape, J.; Vikse, K. L.; Janusson, E.; Taylor, N.; McIndoe, J. S. *Int. J. Mass Spectrom.* **2014**, *373*, 66−71.

(15) Pike, S. D.; Pernik, I.; Theron, R.; McIndoe, J. S.; Weller, A. S. *J. Organomet. Chem.* **2015**, *784*, 75−83.

(16) Klabunde, W. U.S. Patent No. 2,492,048, 1949.

(17) Robertson, R. A. M.; Poole, A. D.; Payne, M. J.; Cole-Hamilton, D. J. *Chem. Commun.* **2001**, *1*, 47−48.

(18) Hooper, J. F.; Chaplin, A. B.; González-Rodríguez, C.; Thompson, A. L.; Weller, A. S.; Willis, M. C. *J. Am. Chem. Soc.* **2012**, *134*, 2906−2909.

(19) (a) van Leeuwen, P. W. N. M.; Chadwick, J. C. *Homogeneous Catalysis*; Wiley-VCH: Weinheim, 2011. (b) Do, L. H.; Labinger, J. A.; Bercaw, J. E. *ACS Catal.* **2013**, *3*, 2582−2585. (c) Albahily, K.; Koç, E.; Al-Baldawi, D.; Savard, D.; Gambarotta, S.; Burchell, T. J.; Duchateau, R. *Angew. Chem., Int. Ed.* **2008**, *47*, 5816−5819. (d) Castellanos-Páez, A.; Castillón, S.; Claver, C.; van Leeuwen, P. W. N. M.; de Lange, W. G. J. *Organometallics* **1998**, *17* (12), 2543−2552.

(20) Pawley, R. J.; Huertos, M. A.; Lloyd-Jones, G. C.; Weller, A. S.; Willis, M. C. *Organometallics* **2012**, *31*, 5650−5659.

(21) Ghosh, R.; Zhang, X.; Achord, P.; Emge, T. J.; Krogh-Jespersen, K.; Goldman, A. S. *J. Am. Chem. Soc.* **2007**, *129*, 853−866.

(22) von Delius, M.; Le, C. M.; Dong, V. M. *J. Am. Chem. Soc.* **2012**, *134*, 15022−15032.

(23) Zuidema, E.; Escorihuela, L.; Eichelsheim, T.; Carbo, J. J.; Bo, C.; Kamer, P. C. J.; van Leeuwen, P. W. N. M. *Chem. - Eur. J.* **2008**, *14*, 1843−1853.

(24) Urtel, H.; Meier, C.; Rominger, F.; Hofmann, P. *Organometallics* **2010**, *29*, 5496−5503.

(25) Kost, T.; Sigalov, M.; Goldberg, L.; Ben-Asuly, A.; Lemcoff, N. G. *J. Organomet. Chem.* **2008**, *693*, 2200−2203.

(26) Patiny, L.; Borel, A. *J. Chem. Inf. Model.* **2013**, *53*, 1223−1228.

DOI: 10.1021/acscatal.6b01489
ACS Catal. 2016, 6, 6911−6917